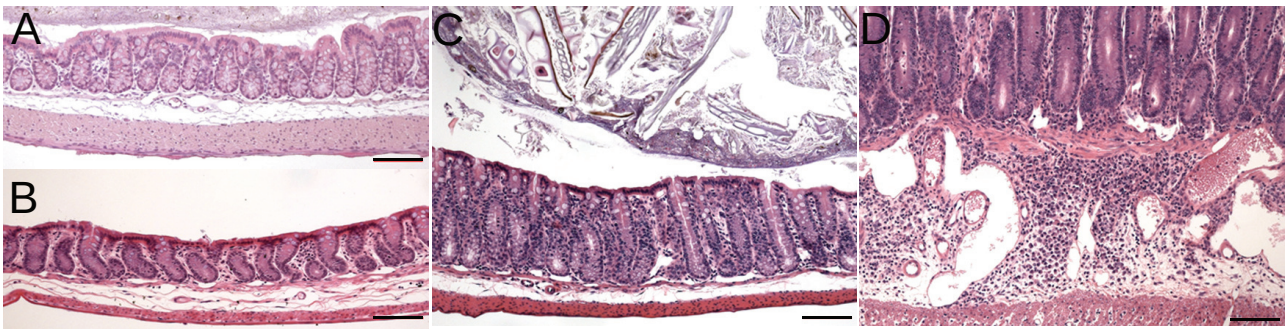

Supplementary Figure S1. Hematoxylin and eosin staining of colon sections from wild-type and *Il10*$^{-/-}$ mice. 7-week–old C57BL/6J wild-type mice (A) and 11-week–old C3Bir wild-type mice (B) did not show any signs of inflammation or lymphatic vessel changes. Colons of 6-week–old B6-*Il10*$^{-/-}$ mice (C) resembled that of wild-type mice whereas colons of 7-week–old C3Bir-*Il10*$^{-/-}$ mice (D) had severe tissue inflammation and enlarged vessels. Scale bars: 100 µm.

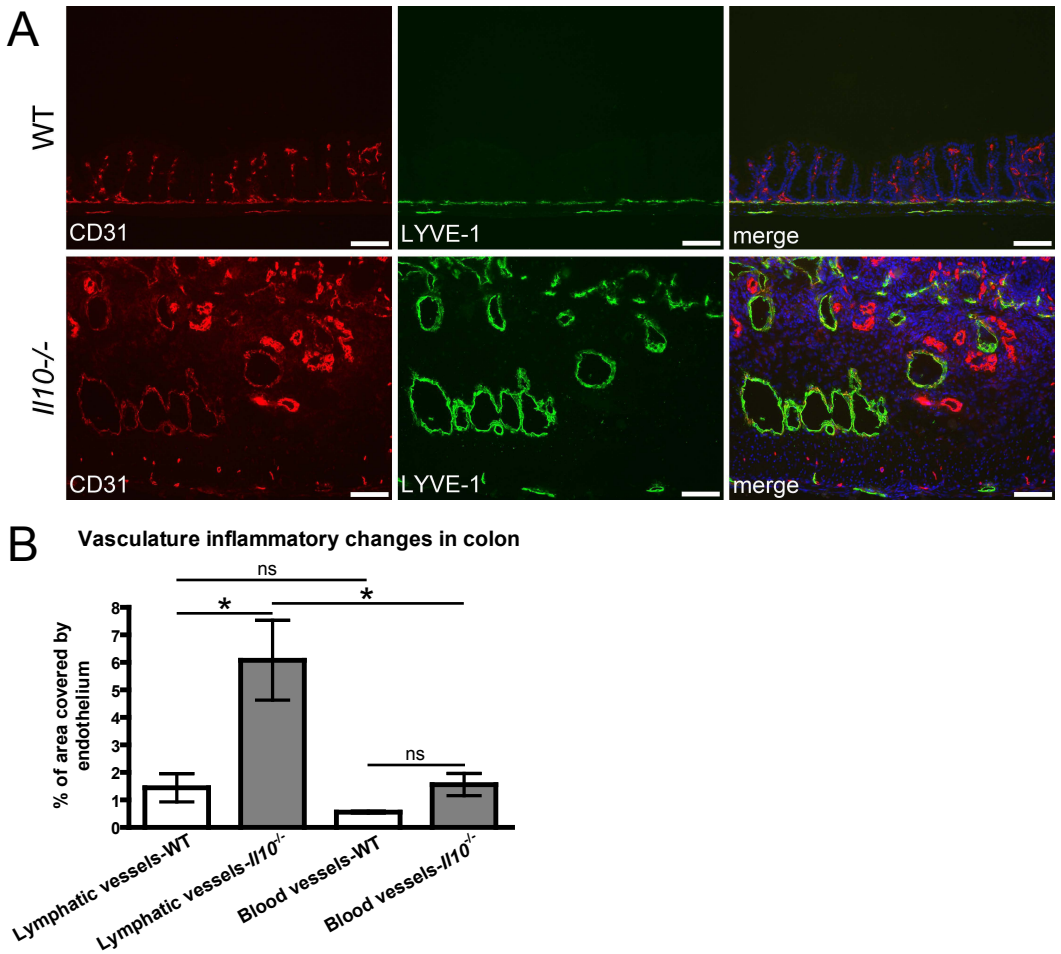

Supplementary Figure S2. Inflammatory lymphatic vessel changes are more pronounced than inflammatory blood vessel changes in *Il10*$^{-/-}$ mouse colon. (A) Representative images of 8-weeks-old wild-type mouse healthy colon tissue and 8-weeks-old *Il10*$^{-/-}$ mouse inflamed colon tissue sections immunostained for LYVE1 (green) and CD31 (red). Scale bars: 100 μm, blue stain: Hoechst. (B) Percentage of areas covered by blood vessel endothelium (CD31^{high}LYVE1^{-}) and lymphatic vessel endothelium (CD31^{low}LYVE1^{+}) were calculated. t-test *p≤0.05 (N per group=3).

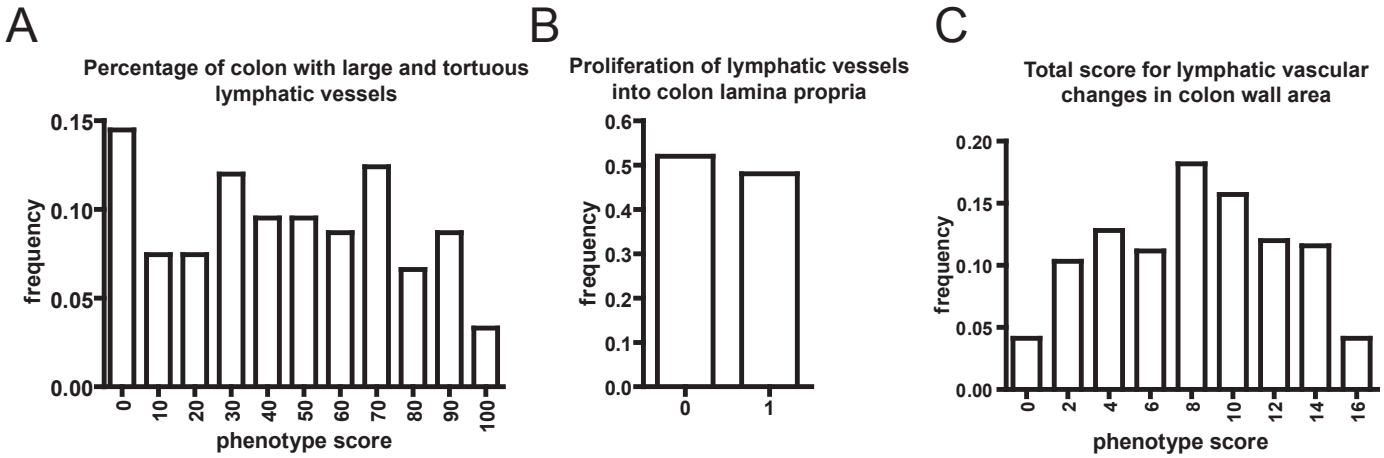

Supplementary Figure S3. Lymphatic vessel traits are approximately normally distributed in F2 *Il10*$^{-/-}$ mice. The analysis was performed considering a normal distribution of all F2 traits, except for the ingrowth of lymphatic vessels into lamina propria (B), which was treated as a binary trait. x-axis: phenotype score, y-axis: percentage of F2 mice with the given phenotype score.

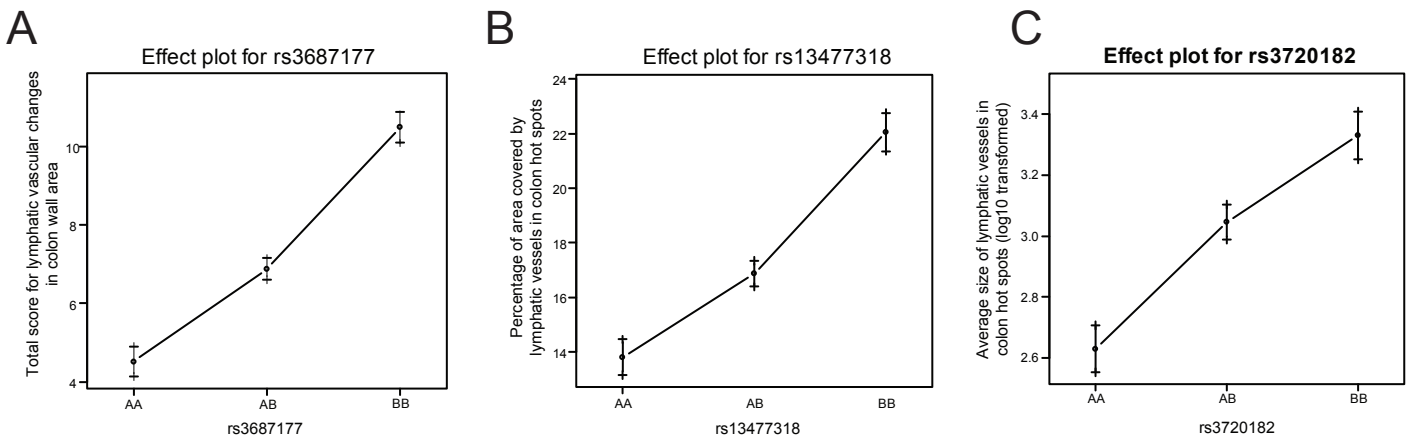

Supplementary Figure S4. Three peak markers with the highest effects on lymphatic vessel inflammatory changes. F2 mice with double C3Bir allele at markers rs3687177 (A), rs13477318 (B) and rs3720182 (C) display the most severe lymphatic vessel subphenotypes. (y-axis: phenotype score, error bars: F2 group variance).

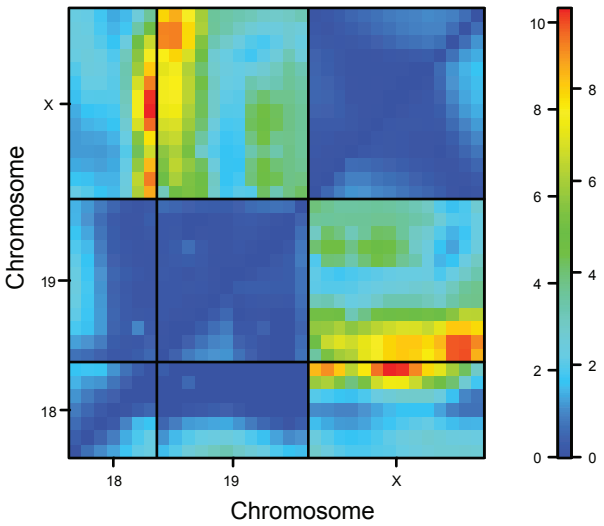

Supplementary Figure S5. Significant interaction is observed between loci on Chromosomes 18, 19 and X. Enlarged view of the two-dimensional genome scan performed with 243 F2 mice and 110 microsatellite markers for the trait: total lymphatic vessel score for non-mucosal intestinal wall area, for the Chromosome pairs X:19 and X:18. The upper left triangle contains the interaction model LOD scores, and the lower right triangle contains the conditional-interactive model LOD scores. Individual colored squares represent markers at the chromosomes indicating the hot spots of interaction. The color bar indicates the LOD scores for the left and right triangles respectively.

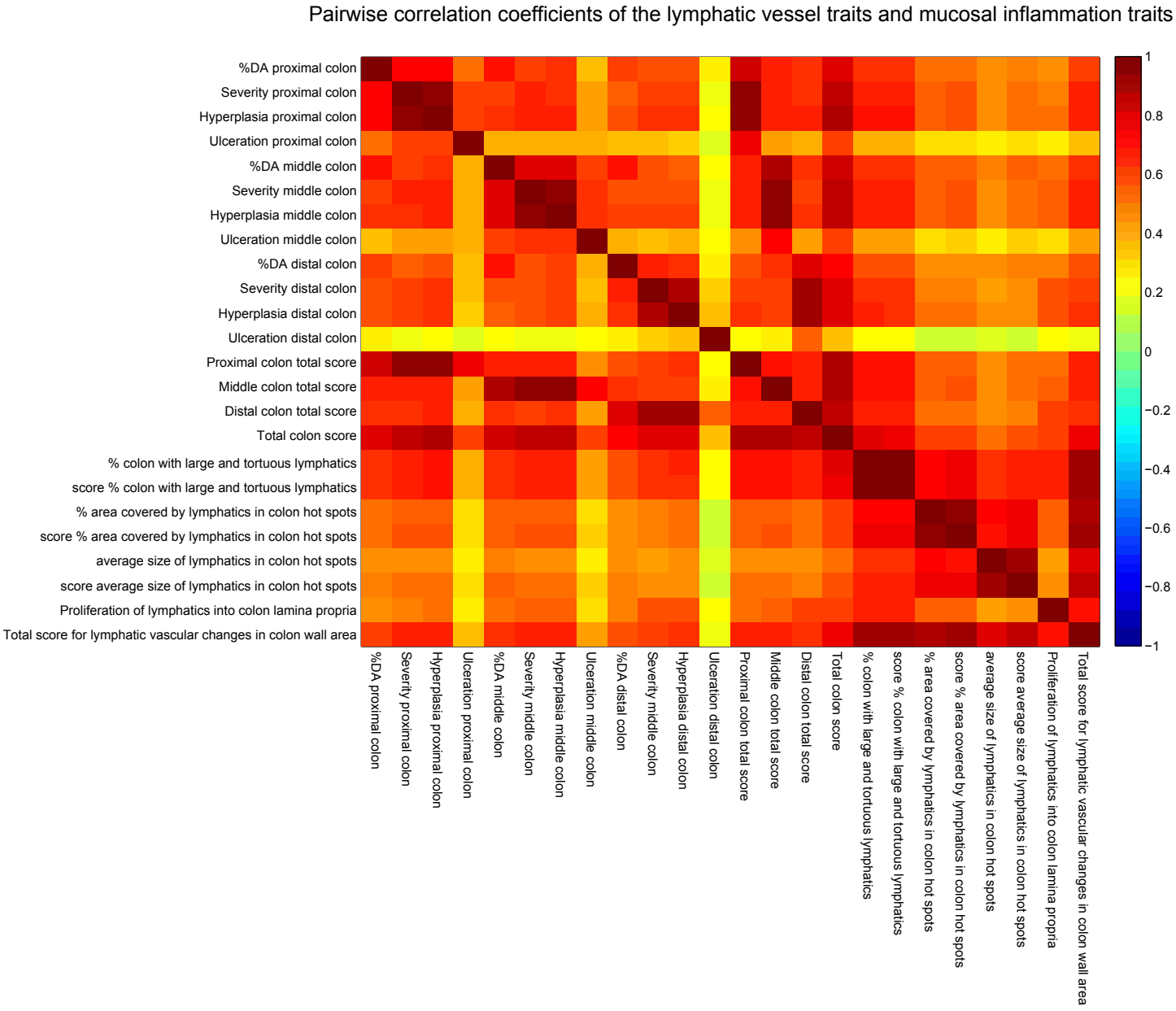

Supplementary Figure S6. The lymphatic vessel traits correlate highly with the mucosal inflammation traits in colitis in *Il10*$^{-/-}$ F2 mice. Matrix visualization for the Pearson pairwise correlation of the lymphatic vessel traits and colitis traits (n= 389 F2 mice). Pearson's correlation coefficients (*r*) were converted into color codes explained by the color bar on the right.

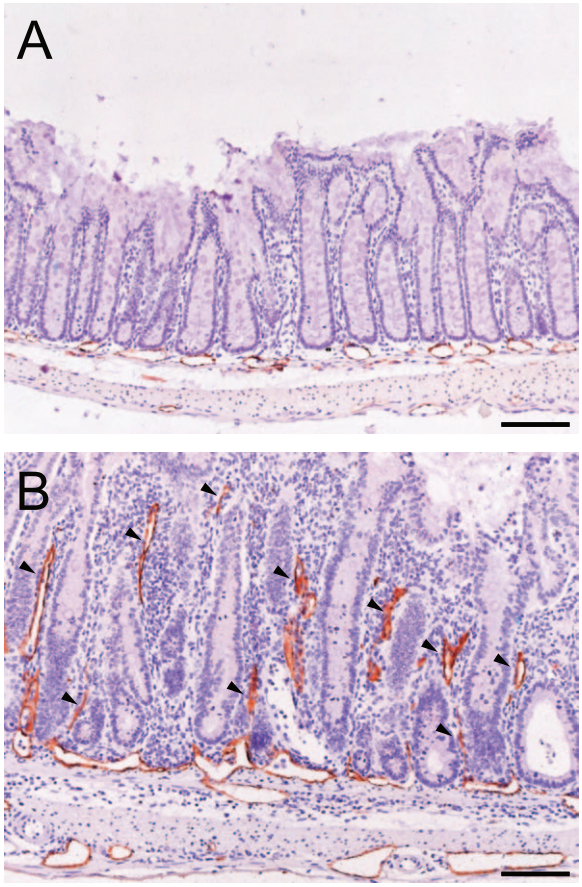

Supplementary Figure S7. Lymphatic vessels invade the colon lamina propria in inflamed tissue. Ingrowth of lymphatic vessels into the lamina propria between the colon epithelial crypts was observed only in inflamed colon. Representative images of normal colon (A) and inflamed colon (B) sections from *Il10*$^{-/-}$ mice, stained for LYVE1 (red), are shown. Arrowheads indicate lymphatic vessels that have grown into the lamina propria. Scale bars: 100 μm.

Supplementary table S1. Scoring system for the lymphatic vessel changes in colitis.

Percentage of whole colon with large and tortuous lymphatic vessels	
Measurement method	**Visual inspection (blinded toward the mouse ID) of paraffin sections stained for LYVE1**
score 0	0%
score 1	1-20%
score 2	21-40%
score 3	41-60%
score 4	61-80%
score 5	81-100%
Percentage of area covered by lymphatic vessels in colon hot spots (3 hot spots chosen per case)	
Measurement method	**IP-LAB software image analysis**
score 0	2.5-10%
score 1	11-15%
score 2	16-20%
score 3	21-25%
score 4	26-30%
score 5	>30%
Average size of lymphatic vessels in colon hot spots (3 hot spots chosen per case)	
Measurement method	**IP-LAB software image analysis**
score 0	<500 μm2
score 1	500-1500 μm2
score 2	1501-2500 μm2
score 3	2501-3500 μm2
score 4	3501-5000 μm2
score 5	>5000 μm2
Proliferation of lymphatic vessels into colon lamina propria (0 or 1)	
Measurement method	**Visual inspection (blinded toward the mouse ID) of paraffin sections stained for LYVE1**
score 0	absence of LYVE-1 positive vessels beyond basis of colon crypts (Figure S7A)
score 1	presence of LYVE-1 positive vessels in lamina propria between the colon crypts (Figure S7B)
Total score for lymphatic vascular changes in colon wall area (0-16)	

Supplementary table S2. Recombination map positions of 110 microsatellite markers used for the genotyping of *Il10*$^{-/-}$ F2 mice. CentiMorgan (cM) positions are reported based on The Jackson Laboratory's online Mouse Genome Informatics (MGI 4.2) resource (http://www.informatics.jax.org).

Microsatellite marker	Chromosome	MGI recombinant map position (cM)	Microsatellite marker	Chromosome	MGI recombinant map position (cM)
D1Mit156	1	32.8	D11Mit140	11	28.0
D1Mit7	1	41	D11Mit36	11	47.6
D1Mit386	1	59.5	D11Mit70	11	54.0
D1Mit100	1	71.5	D11Mit99	11	59.5
D2Mit237	2	28	D11Mit58	11	65.0
D2Mit94	2	47	D11Mit48	11	77.0
D2Mit62	2	65	D12Mit5	12	37.0
D2Mit282	2	83	D12Mit214	12	38.0
D2Mit266	2	109	D12Mit19	12	58.0
D3Mit131	3	4.6	D12Nds2	12	59.0
D3Mit203	3	11.2	D13Mit115	13	11.0
D3Mit212	3	39.7	D13Mit179	13	30.0
D3Mit189	3	49.7	D13Mit11	13	40.0
D3Mit348	3	61.8	D13Mit191	13	45.0
D3Mit19	3	87.6	D13Mit130	13	61.0
D4Mit108	4	12.1	D13Mit260	13	65.0
D4Mit178	4	35.5	D13Mit35	13	75.0
D4Mit187	4	49.6	D14Mit11	14	0.7
D4Mit226	4	78.5	D14Mit44	14	10.0
D5Mit146	5	1	D14Mit141	14	15.0
D5Mit148	5	18	D14Mit203	14	28.3
D5Mit205	5	45	D14Mit193	14	40.0
D5Mit188	5	64	D14Mit165	14	52.0
D5Mit216	5	72	D15Mit179	15	10.8
D5Mit223	5	84	D15Mit138	15	15.4
D6Mit74	6	20.5	D15Mit63	15	29.2
D6Mit230	6	43	D15Mit105	15	47.9
D6Mit15	6	74	D15Mit171	15	54.5
D7Mit152	7	1	D15Mit44	15	59.8
D7Mit247	7	16	D16Mit154	16	3.4
D7Mit213	7	36.9	D16Mit131	16	4.3
D7Mit250	7	37	D16Mit4	16	27.3
D7Mit253	7	52.8	D16Mit139	16	43.1
D7Mit71	7	65.2	D16Mit153	16	56.8
D7Mit332	7	65.6	D16Mit71	16	70.7
D7Mit259	7	72	D17Mit30	17	13.6
D8Mit94	8	13	D17Mit34	17	18.8
D8Mit191	8	21	D17Nds3	17	19.1
D8Mit178	8	33	D17Mit49	17	23.2
D8Mit112	8	53	D17Mit76	17	29.5
D8Mit93	8	72	D17Mit88	17	54.6
D9Mit206	9	20	D18Mit119	18	16.0
D9Mit207	9	33	D18Mit124	18	32.0
D9Mit48	9	34	D18Mit7	18	50.0
D9Mit12	9	55	D19Mit32	19	0.0
D9Mit214	9	62	D19Mit40	19	25.0
D9Mit18	9	71	D19Mit12	19	26.0
D10Mit123	10	4	D19Mit1	19	52.0
D10Mit42	10	44	D19Mit71	19	54.0
D10Mit117	10	48	D19Mit6	19	55.0
D10Mit180	10	64	DXMit124	X	2.8
D10Mit103	10	69.9	DXMit140	X	19.0
D10Mit271	10	70	DXMit149	X	50.0
D11Mit149	11	1	DXMit79	X	50.5
D11Mit236	11	20	DXMit135	X	69.0

Supplementary table S3. 18 SNP markers integrated into the genetic map of Chromosome 3. Physical map (UniSTS annotation of NCBI Mouse Build 37.1) and genetic map (MGI, http://www.informatics.jax.org) were used to estimate the genetic map order of microsatellite markers and SNP markers on Chromosome 3.

Chromosome 3 marker	NCBI Mouse Build 37.1 physical map position (bp)	MGI recombinant map position	Estimated recombinant map position (cM)
D3Mit131	17,462,555	4.6	
D3Mit203	26,835,026	11.2	
D3Mit212	83,121,332	39.7	
rs13459185	95,750,438		47.9
rs13477275	96,140,787		48.1
rs3163371	100,194,280		49.6
D3Mit189	100,779,519	49.7	
rs3720779	101,887,627		50
rs4140272	104,765,253		51.4
rs13477315	106,767,998		53.4
rs13477318	107,918,926		54
rs13477320	108,822,024		54.4
rs3712218	109,572,245		54.8
rs3687751	112,470,201		56.2
rs3716905	113,497,135		56.7
rs3022965	113,722,327		56.9
rs4224164	114,844,526		57.4
rs3687177	116,662,804		58.3
rs3720182	120,471,745		60.2
rs4224200	123,406,475		61
rs3677929	125,568,747		61.5
D3Mit348	126,684,318	61.8	61.7
D3Mit19	157,882,544	87.6	

Supplementary table S4. Results of the low density qPCR array. Genes from the Chromosome 3 QTL interval (approximately 107-128 Mb), endogenous control genes, endothelial and inflammation marker genes are shown with fold change of basal level expression in C3Bir-*Il10*$^{-/-}$ compared to B6-*Il10*$^{-/-}$ mice and Benjamini-Hochberg-corrected p-values.

TaqMan Assay ID	Gene symbol	Fold change	Corrected p-value	TaqMan Assay ID	Gene symbol	Fold change	Corrected p-value
Mm00497922_m1	Ptbp2	1.302	2.31E-01	Mm00438855_m1	F3	1.028	9.24E-01
Mm00499266_m1	Camk2d	1.063	7.12E-01	Mm00833923_m1	Gstm3	0.799	4.50E-01
Mm00804345_m1	Lrrc39	1.368	7.12E-01	Mm00803379_m1	Sars	1.166	4.90E-01
Mm00619360_m1	Wdr47	1.4	1.56E-01	Mm00805036_m1	Arhgap29	1.685	2.31E-01
Mm01324391_m1	Pde5a	1.172	4.90E-01	Mm00660400_m1	Prpf38b	0.969	8.86E-01
Mm00485999_m1	Frrs1	4.076	3.04E-04	Mm00725711_s1	Gstm2	0.664	5.16E-02
Mm00458239_m1	Slc30a7	1.213	2.72E-01	Mm00520420_m1	Slc44a3	1.009	9.52E-01
Mm00463714_m1	6330569M22Rik	1.446	7.65E-02	Mm00512842_m1	Gpsm2	0.88	4.59E-01
Mm00441607_m1	Stxbp3a	1.43	8.51E-02	Mm00492004_m1	Abca4	2.694	5.65E-01
Mm00453178_m1	Ndst3	1.525	1.56E-01	Mm00492394_m1	Gnat2	0.744	2.72E-01
Mm00449197_m1	Vcam1	1.746	2.39E-02	Mm00501651_m1	Dbt	1.084	7.16E-01
Mm00468642_m1	Hiat1	1.147	4.59E-01	Mm00461101_m1	Ahcyl1	0.879	4.59E-01
Mm00435975_m1	Prss12	2.206	8.95E-02	Mm00468111_m1	Dpyd	1.142	5.51E-01
Mm00445066_m1	Vav3	1.317	3.21E-01	Mm00470263_m1	Alg14	0.817	4.59E-01
Mm00432688_m1	Csf1	1.44	2.72E-01	Mm00464291_m1	Dnttip2	0.902	5.58E-01
Mm00483387_m1	Col11a1	1.037	9.01E-01	Mm00457515_m1	Celsr2	0.903	6.18E-01
Mm00613500_m1	Atxn7l2	1.384	2.69E-01	Mm00600213_m1	Bcar3	1.21	3.21E-01
Mm00724102_m1	D3Bwg0562e	1.176	5.58E-01	Mm00622139_m1	Fndc7	1.433	2.04E-01
Mm00525200_s1	Tram1l1	1.492	2.69E-01	Mm00651524_m1	Amy1	0.263	4.59E-01
Mm00508416_m1	Rtcd1	1.01	9.52E-01	Mm00523288_m1	Slc35a3	0.849	2.99E-01
Mm00453144_m1	Ntng1	0.968	9.01E-01	Mm00495930_m1	Ugt8a	1.118	8.11E-01
Mm00431779_m1	Alx3	2.61	5.14E-01	Mm00514644_m1	Edg1	1.159	6.41E-01
Mm00436150_m1	Abcd3	0.798	3.21E-01	Mm00490905_m1	Sort1	1.275	2.04E-01
Mm00498358_m1	Psrc1	1.207	4.95E-01	Mm00519404_m1	Eps8l3	1.025	9.01E-01
Mm00499573_g1	Gstm7	0.85	4.90E-01	Mm00469639_m1	Myoz2	1.347	4.90E-01
Mm00510216_m1	Dph5	0.856	4.59E-01	Mm00485005_m1	Sypl2	1.625	8.95E-02
Mm00833915_g1	Gstm1	0.598	2.39E-02	Mm02342486_mH	Amy2	0.455	6.41E-01
Mm00652377_m1	Palmd	1.078	9.00E-01	Mm00458851_m1	Rnpc3	1.153	4.90E-01
Mm00515890_m1	Gstm5	1.472	1.56E-01	Mm00619261_m1	Tmem56	0.857	3.86E-01
Mm00558495_s1	Gpr61	1.072	8.06E-01	Mm00625784_m1	4921525H12Rik	1.693	3.21E-01
Mm00783337_s1	Cnn3	1.089	6.41E-01	Mm00728197_s1	Gstm4	0.848	2.72E-01
Mm00659237_m1	4921515J06Rik	1.234	5.58E-01	Mm00660744_m1	Sec24d	1.23	5.14E-01
Mm00656783_gH	Gstm6	0.733	1.13E-01	Mm00514996_m1	Gclm	0.949	8.80E-01
Mm00848037_g1	Taf13	1.101	6.41E-01	Mm00509247_m1	2010200O16Rik	1.228	2.72E-01
Mm00554503_m1	Slc25a24	0.996	9.84E-01	Mm00517707_m1	Gpr88	3.035	2.35E-02
Mm00618325_m1	Ank2	1.296	3.21E-01	Mm00508295_m1	1810037I17Rik	0.879	4.90E-01
Mm00557970_m1	Arsj	2.617	6.49E-02	Mm00480767_m1	Ndst4	0.924	7.76E-01
Mm00523781_m1	Clcc1	1.196	3.21E-01	Mm00433188_m1	Fabp2	0.461	1.98E-01
Mm00481738_g1	2510027J23Rik	4.178	8.51E-02	**Endogenous control assays**			
Mm00469621_m1	Extl2	1.129	5.65E-01	Mm02342429_g1	Ppia		
Mm00462236_m1	Fnbp1l	1.121	4.90E-01	Mm00801778_m1	Ifng		
Mm00476778_m1	Usp53	1.034	9.01E-01	Mm01246167_m1	Pecam1		
Mm00462529_m1	Olfm3	0.626	2.69E-01	Mm01222419_m1	Kdr		
Mm00621458_g1	A730020M07Rik	1.309	6.41E-01	Mm00486938_m1	Cdh5		
Mm00491977_s1	Synpo2	1.298	4.90E-01	Mm99999915_g1	Gapdh		
Mm00802671_m1	Gnai3	1.002	9.87E-01	Mm00607939_s1	Actb		
Mm00512072_m1	Ampd2	0.99	9.52E-01	Mm00435617_m1	Pgk1		
Mm00619134_m1	Prmt6	0.932	6.41E-01	Hs99999901_s1	18S rRNA		
Mm00525196_m1	Amigo1	0.899	7.12E-01				